Bachelor Research Project:

Cosmic Radiation and Cosmogenic Isotope Production

Analysis of Atomic Age Radiocarbon Data

Peter Sarkozi
S3101231

Faculty of Science and Engineering
University of Groningen
The Netherlands
2 July 2019

Contents

1 Introduction **2**

2 Radiocarbon Basics **2**
2.1 Carbon Isotopes 2
2.2 Generation and Decay 3
2.3 Carbon Dispersion 3
2.4 Measurement Methods 3
2.5 Presentation of ^{14}C values 4

3 Trends in 14C Data **5**
3.1 Historical 5
3.1.1 Radiocarbon Spikes in the Past 5
3.2 Modern Trends 6
3.3 Expected Variations 6
3.3.1 Seasonal Variations 7
3.3.2 Solar Cycle 7
3.3.3 Solar Events 8
3.3.4 Cosmic Events 9

4 Analysis **9**

5 Results **12**
5.1 The Modern Suess Effect 12
5.2 Detection of the Solar Cycle 12
5.3 Final Residuals 13
5.4 Summary 16

6 Discussion and Conclusions **20**
6.1 Discussion 20
6.2 Conclusions 20
6.3 Acknowledgements 21

7 Appendix **25**

1 Introduction

Radiocarbon (^{14}C) is a naturally occurring unstable isotope of carbon used in various scientific disciplines such as archaeology, meteorology, biology, and geology. Its common occurrence on the surface of Earth makes it a reliable tracer for natural processes and its half life of a little under 6000 years makes it an excellent dating tool when it comes to early civilizations. Thanks to its multidisciplinary usefulness it has been studied extensively, but being a mainly archaeological tool, much of the effort has been focused on building a reliable database for age calibration (INTCAL, see Section 3.1). From the 60's several research groups started conducting regular atmospheric radiocarbon measurements, and due to their efforts today we have reliable, high-resolution radiocarbon datasets. The goal of this project is to examine these datasets, identify short-term variations (seasonal changes, the solar cycle), and see whether the datasets are influenced by any extra-terrestrial effects (e.g. cosmic events). Researching this is justified by the following:

- Historical radiocarbon datasets usually have no better than yearly resolution, obscuring short term changes. Recent, high-resolution data can help us better characterize and understand the origin of ^{14}C fluctuations.
- Study of radiocarbon can lead to new information on cosmic events, such as shining a light on past occurrences and resolving their intensities. Section 3.1.1 describes two radiocarbon events in the past, the origins of which are still debated.

2 Radiocarbon Basics

2.1 Carbon Isotopes

Carbon is present in the biosphere in large quantities, being the basic building block of all life. Furthermore, the atmosphere (CO_2, CH_4, volatile organics) and the hydrosphere (H_2CO_3, HCO_3^-, CO_3^{2-}, DOC) both contain considerable quantities of carbon compounds. These, together with the carbon deposits of the lithosphere form a quasi-closed system, with C being transported within and across these reservoirs by various processes (many of which are biologically driven). These processes are collectively referred to as the carbon cycle [1]. Carbon ($Z = 6$) has three naturally occurring isotopes. The most common is ^{12}C, with an abundance of 98.89%. The other 1.11% is ^{13}C. These isotopes are stable. ^{14}C, commonly referred to as radiocarbon, occurs in trace amounts only: it is unstable with a half-life of 5730 ± 40 years [2]. Sometimes the physically less accurate Libby half-life of 5568 years is used in calculations [3]. The loss from decay is at least partially compensated by production in the atmosphere. Being an unstable naturally occurring isotope that is constantly exchanged, deposited and frequently trapped by natural processes, radiocarbon can be used as a natural dating tool. In 1960 Willard Frank Libby was awarded the chemical

Nobel prize for conceptualizing this, formally "for his method to use carbon-14 for age determination in archaeology, geology, geophysics, and other branches of science". [1]

2.2 Generation and Decay

Radiocarbon is formed when cosmic rays (particles in the GeV energy range) hit the Earth, interact with O and N, and release free neutrons making a $^{14}N(n,p)^{14}C$ reaction possible. ^{14}C then breaks down by β^- decay [1]. Libby, in his 1960 Nobel lecture [4] estimated the expected activity of fresh biospheric carbon, the estimate being within 10% error of the later measured value. He assumed equilibrium between the two processes. He further conducted carbonate and bicarbonate measurements in deep ocean waters giving evidence that cosmic ray bombardment of Earth has been constant over a long time (thousands of years).

2.3 Carbon Dispersion

Through ^{14}C both short- and long-term transport phenomena can be studied reliably (as long as the limited lifetime of radiocarbon allows this). Examples include the global atmospheric mixing, the existence of which has been analysed through the study of the so called bomb peak (see Section 3.2), and the estimation of deep oceanic mixing timescales [4]. For this project, the former is much more relevant: the mixing time between the Northern and Southern Hemispheres is 1-2 years [5].

2.4 Measurement Methods

Since the discovery of radiocarbon dating, different methods have been developed to measure the ^{14}C content of samples. The problem is far from trivial; the low ^{12}C :^{14}C ratio ($\approx 1 : 10^{-12}$), the low energies of emitted electrons in the decay process (156 keV at most) and the overlap of the decay's energy spectrum with that of ^{222}Rn's and ^{3}H's make matters rather difficult. Three types of measuring processes are commonly encountered in the field.

- *Gas proportional counting* is the measurement method presented by Libby [4] in his Nobel lecture, originally pioneered by Hessel de Vries. In the modern version of the process, a sample is combusted to produce CO_2. ^{222}Rn which has a half life of only a few days is eliminated by storing the sample for about a month, then the CO_2 is pressurized in a tube. A high voltage is applied, so that a decay causes an ionization trail and an electric pulse can be measured.

- In the process of *liquid scintillation spectrometry* once again CO_2 is obtained by combustion. This is then turned into a carbon-rich liquid, benzene (C_6H_6). Once again, radon is allowed to decay. Finally the sample

is loaded into a low-potassium vial, and a phosphoric scintillant (butyl-PBD) is dissolved in it. Through reaction with the scintillant, β^- decays cause photon-emissions.

Both methods presented above rely on the decay of ^{14}C for measurements. They necessitate shielding, such as a physical barrier (passive shielding) or active monitoring of the background radiation to filter out its effects.

- *Accelerator mass spectrometry* (AMS) is an approach which doesn't rely on the activity of the sample, and therefore permits much smaller sample sizes. Meijer et al. (2006) reported achieving combined uncertainties of ±3‰ using AMS, and note that this is comparable to the practical limits of regular proportional counter measurements (±2-3‰). Given that there are numerous sites worldwide collecting regular air samples in quantities smaller than what is required for proportional counter measurements but large enough for AMS, this poses the prospect of greatly expanding existing radiocarbon databases [6].

For a more detailed, illustrated treatment of the measurement processes, see Bayliss et al. [7].

2.5 Presentation of ^{14}C values

To characterize a sample, the simplest approach is to simply determine the ratios of carbon isotopes. But given the extremely low ^{12}C :^{14}C ratio, and that traditionally the directly measured values were activities, in addition to other physical and historical factors, radiocarbon values are reported in a more complicated manner. In 1977 Stuiver and Polach [3] recommended a standard manner in which radiocarbon values should be reported to avoid ambiguities, based on the field's already established practices. The most important points are presented below.
Activities are compared to that of an archived oxalic-acid sample (or a derived substandard), based on the activity of the sample in AD 1950. Radiocarbon results used for dating are reported with units 'years BP' (Before Present), where the present is considered to be AD 1950.
There are two different corrections described in the paper in question, and based on whether they are taken into account when values are reported, four distinct symbols are used. One correction arises from the different uptake of carbon isotopes in biological and chemical processes, originating in the mass difference of the isotopes in question. This is referred to as isotopic fractionation. Since ^{13}C is also affected by a mass difference, one can use it as a reference to normalize for this effect [7]. The other correction is in the activity of radiocarbon: historically the Libby half-life of 5568 years was used, which may be corrected to the more accurate 5730 year value. Age corrected values are represented by Greek deltas, values based on the Libby half-life are denoted by latin d-s. If the value is corrected for fractionation, a capital letter is used. Most studies in dating and environmental research today take fractionation into account.

$d^{14}C$	Libby half-life used, not corrected for fractionation
$D^{14}C$	Libby half-life used, corrected for fractionation
$\delta^{14}C$	5730 yr half-life, not corrected for fractionation
$\Delta^{14}C$	5730 yr half-life, corrected for fractionation

Table 1: Commonly reported radiocarbon values.

3 Trends in 14C Data

3.1 Historical

Historical ^{14}C data is provided by the IntCal [8] dataset. A 5-year resolution is available for the last 14,000 years (as of IntCal13) based on measurements performed on tree-rings. Older values are also provided, back to approx 50,000 BC, but these are based on other measurement methods that also carry significant errors in sample age (e.g. coral measurements) [9].

3.1.1 Radiocarbon Spikes in the Past

Anomalous increases in atmospheric radiocarbon have been detected through annual tree-ring measurements for the years 744-775 AD and 993-994 AD.
The former has been confirmed using various tree-ring measurements, namely two Japanese cedar trees [10], oak from Germany, and New Zealand kauri trees [11], all consistent with IntCal data. A peak in the production of another cosmogenic isotope, ^{10}Be was also observed through the study of ice core layers, however, the dating of such layers is generally less reliable than dendrochronology. In the Japanese data, a 12‰ (7.2σ) increase in ^{14}C content was observable within a single year, followed by a decrease lasting several years. Through a simulation, Miyake et al. also determined that the the duration of the increase was likely less than 1 year [10]. AMS measurement of New Zealand tree-rings (Güttler et al.) showed a jump of 14‰ in AD 775, with a further 5‰ increase until the end of AD 776. The authors claim that the gradual increase can be explained by delayed exchange between the troposphere and the stratosphere, assuming dominantly (70-80%) stratospheric radiocarbon production with a mean residence time of 2 years. The decline observed was similar to Northern Hemisphere results (lasting until AD 783). Ultimately, the event is estimated to have increased the yearly production of radiocarbon to 2.5-10 times its regular value for the year of the event [11].
The AD 993-994 event (originally reported as AD 992-993, and later corrected) was studied by Miyake et al. through tree-ring measurements performed on two Japanese trees (Yaku cedar from Yaku Island and Hinoki cypress from Iida city), and ^{10}Be data obtained from the Dome Fuji ice core in Antarctica. The trees showed increases of 9‰ and 11.3‰ (5.1σ and 6.5σ confidence levels respectively) [12] [13]. The corresponding annual production is estimated to be 1.8 ± 0.2 times its usual value [14].
Tree-ring data for the periods of these two events has since been gathered

through a global collaboration (COSMIC) including 44 tree-ring measurement sites on five continents, representing most of Earth's extra-tropical forests. The obtained results were consistent with the original ones from Japan, New Zealand and Europe [14].
The cause of the peaks has not been conclusively established so far. Various possible sources (mainly cosmic events, such as solar storms, comet impacts or supernovae) have been discussed, but the magnitudes of the peaks generally seem to be larger than what we'd expect from such events. See Section 3.3 for details.

3.2 Modern Trends

Increased anthropogenic influences introduced rapid changes into the atmospheric radioisotope levels. Two major influences are commonly mentioned. First, atmospheric nuclear testing in the 50's and early 60's caused a sharp increase in atmospheric radiocarbon content, almost doubling the $^{14}C/C$ ratio. The rapid climb of ^{14}C levels was ended by the Partial Nuclear Test Ban Treaty in 1963, resulting in a peak of radiocarbon levels around this year. After this, the levels decreased almost exponentially due to the exchange with other carbon reservoirs (oceans and biosphere). The peak is now commonly referred to as the bomb curve. Second, fossil fuel emissions dilute the radiocarbon content of the atmosphere by adding CO_2 that is essentially free of radiocarbon. This phenomenon, described by Suess in 1955 [15], is called the Suess effect. The atmospheric radiocarbon levels were governed mainly by the bomb curve until the 1990s, with the fossil fuel effect gradually becoming more relevant. In the 21st century, the Suess effect became the principal driving force behind the general radiocarbon trend. It is estimated that emissions deplete ^{14}C content by 12-14 ‰ per year, which is partially compensated for by industrial and natural ^{14}C production and release from the biosphere [5]. Indeed, from atmospheric measurements one can observe a smaller decrease of approx. 4-4.5 ‰ per year (obtained from the Lutjewad and Jungfraujoch datasets, see Section 5.1).

3.3 Expected Variations

The presence of variations in ^{14}C levels due to environmental phenomena has been well established. We already discussed some of these: the AD 775-776 and AD 993-994 spikes, the bomb curve, and the Suess effect. While the latter are well understood, the origins of the first two are yet to be determined. Numerous hypotheses exist, some of which are presented below. Furthermore we discuss two short-term, periodic changes that we expect to see in the radiocarbon data during our analysis: the seasonal changes and the changes corresponding to the solar cycle.

Measurement site	Seasonal peak-to-trough variation in ‰
Point Barrow	12.0 ± 1.5
Fruholmen	12.5 ± 2.2
Jungfraujoch	6.4 ± 0.6
Izaña	6.6 ± 1.6
Wellington	Not Significant
South Pole	5.0 ± 1.2

Table 2: Seasonal variations presented in the paper of Meijer et al [6] (see the original sources therein). This table was adapted from the cited paper.

3.3.1 Seasonal Variations

Historical data is usually based on tree-ring measurements, which can provide at most two data points per year (for that the difference between NH and SH growth seasons has to be exploited). In contrast, this project focuses on recent, more frequent atmospheric measurements. The presence of seasonal variations in ^{14}C has been well established, for example, in the work of Meijer et al. [6] several seasonal fits are presented. These are in Table 2.

3.3.2 Solar Cycle

Sunspots are continuously appearing and disappearing dark regions on the surface of the Sun, observable in the visible spectrum. They are commonly used to approximate solar activity, and have been subjects of interest for several hundred years: thanks to this, today we have a reliable long-term record (≈ 300 years) of sunspot numbers. The solar cycle (Schwabe cycle) traces the variation in the number of sunspots with an approximately 11 year periodicity. Rudolf Wolf introduced a measure (known as the Wolf number) for sunspots, defined as ten times the number of sunspot groups plus the number of individual sunspots; possibly multiplied by a constant factor depending on observational conditions. The Wolf number simply characterizes the total number of sunspots [16]. The solar cycle modulates the flux of galactic cosmic rays through changing the interplanetary magnetic field. This means that what we're trying to approximate using Wolf's number in the case of radiocarbon is the Sun's magnetic activity. It is known that the Sun also exhibits an approximately 22-year long magnetic cycle (Hale cycle), which corresponds to its reversal of magnetic polarity. In fact, changes in ^{14}C can be (and are) used to reconstruct the solar activity before direct observations became common. Note that direct sunspot observations are generally considered to be better indicators of solar activity when available. However, it has been shown through radiocarbon analysis that the magnetic cycles of the Sun were still present during past solar minima (Spörer and Maunder minima) when the sunspot activity was very weak [17]. There is a clear anticorrelation between atmospheric cosmic ray intensity on Earth and the Wolf number. As one would expect then, ^{14}C shows a peak during the Maunder and Dalton minima. Other grand solar minima (such as the Spörer

Samples	1903-1913	1913-1923	1923-1933	1933-1944
Wines	4.0 ± 0.8	4.3 ± 0.8	4.5 ± 0.9	4.3 ± 0.8
tree-rings		1.5 ± 0.5	2.1 ± 0.5	2.0 ± 0.5

Table 3: Amplitudes in radiocarbon data associated with the solar modulation. This table was reproduced from the work of Povinec et al. [20].

Reference	Sample type	Investigated interval	Periodicity (y)	Av. t shift (y)	Amplitude (‰)
Baxter & Walton (1971)	Whiskies	1925-1954	11 ± 1	4	7.2 ± 4.9
Damon, Long & Wallick (1973)	Tree-rings	1940-1954	10 ± 1	4	2.1 ± 1.0
Povinec	Tree-rings	1932-1952	10 ± 1	3	3.1 ± 1.2
Burchuladze et al. (1980)	Wines	1909-1952	11 ± 1	4	4.3 ± 1.6
Stuiver and Quay (1981)	Tree-rings	1916-1954	12 ± 1	4	1.9 ± 0.8

Table 4: Amplitudes and time shifts (between the Schwabe cycle and its effect on radioisotope levels) in ^{14}C data found by different groups, presented by Povinec et al. [20]. This table was copied from the paper in question.

minimum) were reconstructed from ^{14}C values [18]. In contrast to the seasonal changes, a period of 11 years can already be detected in tree-ring measurements with an annual resolution. Friedrich et al. [19] observed changes with period 9-11 years and amplitude 1.5-3‰ in the ^{14}C content of 3rd-5th century rings of two European (Scandinavian and eastern German) trees.
Povinec et al. [20] present several detections of the solar cycle in tree-rings and alcohol. These results are presented in Tables 3 and 4. Note that even for the same solar cycle, different groups obtained contradictory results. Burchuladze et al. [21] obtained an average amplitude of 4.7 ± 0.5‰ from Slovakian tree-rings and Georgian wines, observing an average time-shift of 3.5 years for the anti-correlation with the solar cycle, and noting that the anti-correlation is more clearly observable for single cycles.
Masuda et al. showed using wavelet analysis that the Hale cycle is also detectable in ^{14}C values. In the period 1620-1740 the obtained amplitudes were in the range 1-3 ‰ [18].

3.3.3 Solar Events

Concerning the AD775 and AD933 events, the possibility of a large solar proton event (SPE) causing a sharp spike in radiocarbon production has been proposed. First estimates of how large an actual SPE would have to be to cause the spikes in question led to the initial rejection of the SPE hypothesis [10], but later, reduced estimates became more acceptable. Furthermore reliable records of contemporary auroras have since been discovered, partially supporting the SPE hypothesis [22]. Nevertheless, SPEs having a direct and pronounced effect on radiocarbon ratios is yet to be confirmed. The largest known such event, which occurred in AD 1856, could not be observed in ^{14}C data [23].

3.3.4 Cosmic Events

Cosmic particle events in general can have an influence on radiocarbon production. Supernovae or large flares from magnetars (soft gamma repeaters (SGRs) or anomalous x-ray pulsars (AXPs)) could in theory have an observable effect. Neuhauser et al. give estimates of the required energies for the events to be observable in the context of the AD775 peak [24]. As the main goal of this project is data analysis, these estimates are not explored here in detail.

4 Analysis

In the framework of this project, nine radiocarbon datasets have been analyzed: eight of which are publicly available online [25], and one (Lutjewad) comes from the University of Groningen. As this project aimed at analyzing data from the 20th century, the Suess effect and the bomb peak had to be eliminated. To circumvent the difficulties of finding a mathematical expression that would describe these effects, short (10-25 year) periods were selected from the data sets, so that the bomb curve could be approximated by a simple polynomial. By examining residuals, it was deemed that a second order polynomial was the simplest one sufficient for this purpose. See Figure 1a for example: the residuals should not show any coherent non-periodic structure, which is clearly not the case for a linear fit. Ideally one would test the longest possible period to utilize all the available data, but in practice we chose to use the length one or two solar cycles, for the following reasons:

- Solar cycles are not exactly of the same length, and solar activity (inferred from sunspot numbers) varies between cycles. This makes fitting a curve to the solar cycle more complicated if more cycles are included.
- The bomb peak is a very sharp anomaly that had to be avoided to get an acceptable fit, thus we excluded the 1960s from the analysis. See Figure 1c for justification. This significantly shortened the spans of four data sets.

Curve fitting was carried out in Wolfram Mathematica (v. 11.3.0.0), relying on Mathematica's FindFit [27] function. This function returns locally optimal values for unknown parameters in a model function. Local optimality, however, means that the parameter values found do not necessarily provide an acceptable fit. This problem had to be resolved by iterating over a large array of initial guesses for the parameters, and examining the residuals. An appropriate measure for the quality of the fit is the sum of all residuals-squared (although with this simple method we cannot compare fits between different data sets given the different number of data points).
All data sets were essentially processed in the same way, described below:

1. If needed, measurement dates were converted to decimal format. For measurements carried out over a given time interval, the start and end dates were averaged.

Measurement site	A.m.f.	Period covered	^{14}C value used	Location	Altitude (m asl)
Point Barrow	12.8/y	1985.2-1991.9	Δ14C	Alaska	11 [6]
South Pole	9.7/y	1984.8-1992.0	Δ14C	Antarctica	2810 [6]
Jungfraujoch	12.0/y	1986.5-2016.1	Δ14C	Switzerland	3450 [6]
Schauinsland	23.3/y	1978.0-1997.0	D14C	Germany	1205 [25]
Vermunt	15.0/y	1959.1-1983.4	D14C	Austria	1800 [25]
Wellington	9.4/y	1955.2-1993.5	D14C	New Zealand	low [6]
Fruholmen	16.9/y	1963.0-1993.5	Δ14C	Norway	70 [6]
Izaña	10.5/y	1963.2-1990.9	Δ14C	Tenerife, Canary Islands	2376 [6]
Lutjewad	11.4/y	2003.0-2017.5	Δ14C	The Netherlands	low [26]

Table 5: Radiocarbon datasets used in this project. The second column shows the average measurement frequency.

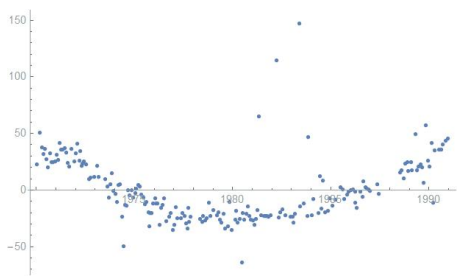

(a) Residuals from the Wellington data set, years 1970 to 1990, obtained with a linear fit.

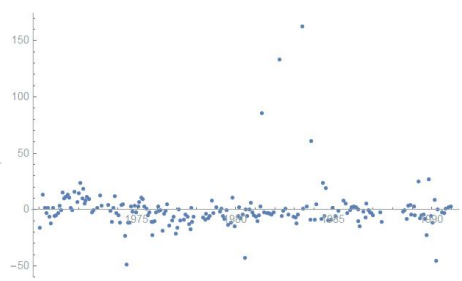

(b) Residuals from the Wellington data set, years 1970 to 1990, quadratic fit.

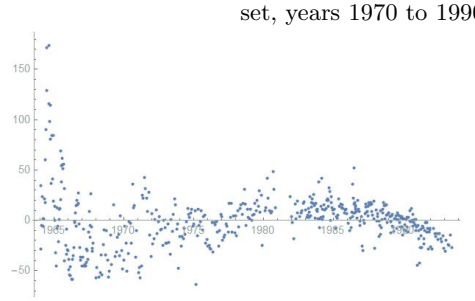

(c) Residuals from a quadratic fit to the Fruholmen data, 1964 to 1993.

Figure 1: Linear and quadratic residuals of certain datasets, justifying the use of a quadratic fit.

2. A quadratic curve of the form $Ax^2 + Bx + C$ was used to approximate the trend in the used data set.

3. The most extreme values (based on the residuals with respect to the first quadratic fit), deemed to be either outliers or other non-periodic events, were discarded temporarily. The value beyond which others were discarded was set in terms of the standard deviation (σ) of the first-fit residuals. The multiplier for this was set based partly on personal judgment, as the outliers themselves would have an effect on the initial fit and σ anyway. Nevertheless, it was always either 3 or 4, to avoid unjustly discarding values.

4. Once the outliers were discarded, we fitted two more models to the reduced datasets. One of the form $Ax^2+Bx+C+A_1\sin(\omega_1 * x+\phi_1)$, and one of the form $Ax^2+Bx+C+A_1\sin(\omega_1 * x+\phi_1)+A_2\sin(\omega_2 * x+\phi_2)$ (the previously obtained values for the parameters were *not* carried over). These models were chosen so that we could approximate the seasonal and solar-cycle based variations (if present) in the data by sine waves superimposed on the general trend. Ultimately, all three components should be independent.

5. If acceptable fits with the expected periods are found, these are eliminated from the original data set (the one before the removal of outliers), yielding a new set of residuals. Acceptability of a fit is evaluated based on three criteria:

   (a) Periods are supposed to be physically meaningful, that is, either correspond to the solar cycle ($\omega \approx 2\pi/11$) or seasonal variations ($\omega \approx 2\pi$).

   (b) The sum of the residuals squared should be significantly lower than for most fits. This can be checked graphically by plotting the list of the residuals squared for all the fits found by Mathematica.

   (c) The amplitudes of the sine fits shouldn't be too small or too large. Section 3.3 describes what amplitudes we expect approximately.

   Note that if no good double sine fit is found, a single sinusoidal fit will be considered instead (also subject to the criteria above).

6. The final set of residuals is examined in an attempt to find peaks or other deviations, possibly corresponding to environmental events.

Finally, note that because of the simplicity of our model and because we are only looking at physically meaningful results we do not run the risk of overfitting. The sums of residuals squared sufficiently characterize the fits: the lower value we get, the better the fit is. As mentioned before, we only compare these values for different obtained fits within the same dataset.

Site	Period Analyzed	Fit found	SM	PR	Frequency in rad/y (period)	Amplitude
Wellington	1968-1992	Single	3	4	$\omega = 0.606$ (10.4 y)	$A = 5.691$‰
Fruholmen	1970-1990	Double	4	1	$\omega_1 = 0.480$ (13.1 y), $\omega_2 = 6.271$ (1.0 y)	$A_1 = 5.57$‰, $A_2 = 9.382$‰
Izaña	1980-1990	Single	4	0	$\omega = 5.598$ (1.1 y)	$A = 4.035$‰
Schauinsland	1977-1996	Double	3	6	$\omega_1 = 0.516$ (12.2 y), $\omega_2 = 6.282$ (1.0 y)	$A_1 = 4.562$‰, $A_2 = 5.206$‰
Lutjewad	2003-2017	Single	4	0	$\omega = 6.283$ (1.0 y)	$A = 6.733$‰
Jungfraujoch	1986-2015	Double	4	0	$\omega_1 = 0.574$ (10.9 y), $\omega_2 = 6.278$ (1.0 y)	$A_1 = 3.382$‰, $A_2 = 2.228$‰
Vermunt	1968-1982	Single	3	1	$\omega = 6.289$ (1.0 y)	$A = 6.667$‰
South Pole	1984-1991	Single	4	0	$\omega = 6.427$ (1.0 y)	$A = 2.203$‰
Point Barrow	1985-1991	Single	4	0	$\omega = 6.311$ (1.0 y)	$A = 4.975$‰
Wellington*	1968-1992	Double	3	4	$\omega_1 = 0.588$ (10.7 y), $\omega_2 = 0.997$ (6.3 y)	$A_1 = 5.016$‰, $A_2 = 4.435$‰
Vermunt*	1968-1982	Double	3	1	$\omega_1 = 0.948$ (6.6 y), $\omega_2 = 6.286$ (1.0 y)	$A_1 = 11.592$‰, $A_2 = 6.154$‰

Table 6: Analyzed periods and found fits. If a double fit is found, the frequencies and amplitudes are denoted by subscripts one and two. SM expresses beyond how many sigmas values were considered outliers/peaks with respect to the initial quadratic fit, and PR is the number of temporarily discarded values. Frequencies can be converted to periods using $T = 2\pi/\omega$.

5 Results

In this section, the results of the analysis are presented. See Table 6 for the fits found. For each combination of site and period, the four best fits were examined (first for double, then for single fits), and evaluated based on the requirements described in the previous section. If a good double sine fit (seasonal and solar cycle) is found, only that is presented. Otherwise the best single sine fit is given.

5.1 The Modern Suess Effect

Although it is a trivial matter, we estimated the decrease in 21st century Δ^{14}C levels assuming a linear trend. For this we used the data from Jungraujoch (2003-2015) and Lutjewad (2003-2017). The results from a linear fit in Mathematica were -4.5‰ per year and -4.1‰ per year respectively.

5.2 Detection of the Solar Cycle

Periodic variations in radiocarbon corresponding to the Schwabe cycle were found in four cases: the three double sine fits and Wellington. Figure 2 shows the correspondence between the found fits and the Wolf number. In section 3.3.2 it was mentioned that while there is a clear link between the Wolf number and atmospheric radiocarbon levels, the bomb peak in the 60's and the changing length of cycles complicate the testing of this relationship significantly. While fitting a periodic function onto the observed Wolf numbers might be possible, the changing length makes this approach overly general and quite error prone. Instead, we base our conclusions on observing the features of Figure 2 directly,

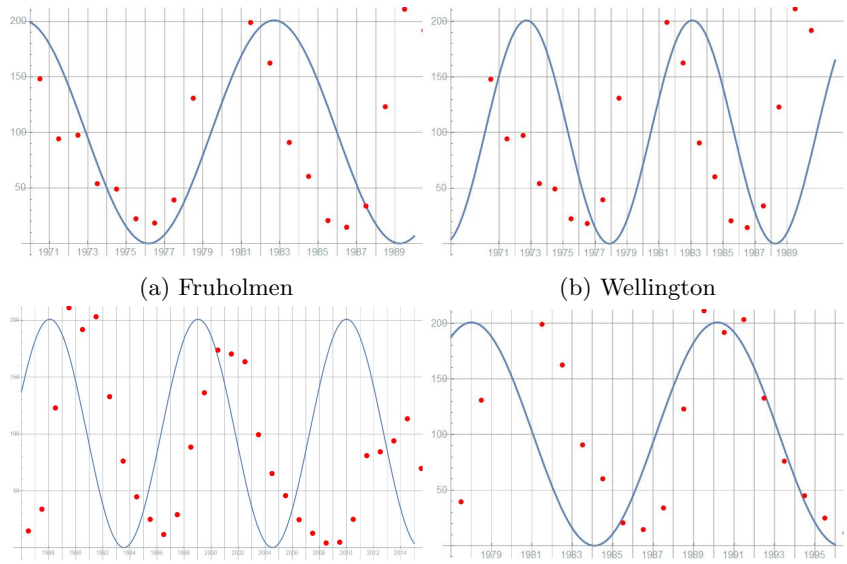

(a) Fruholmen (b) Wellington

(c) Jungfraujoch (d) Schauinsland

Figure 2: Solar offsets for the datasets where the Schwabe cycle was found. The blue lines correspond to the solar component of the obtained fit, with modified amplitudes and vertical offsets for easier comparability. The red dots show variations in the Wolf number for the period in question.

without resorting to any complicated mathematical analysis. First, note that there is a clear anticorrelation between the Wolf number and the atmospheric neutron flux induced by cosmic rays [28]. Thus we expect radiocarbon production to peak during the solar minimum, and production should be suppressed during the maximum. The simplest assumption is that the peaks and troughs in the Wolf number correspond to the following troughs and peaks (respectively) in radiocarbon. Table 7 shows the obtained results (read from Figure 2), along with a set of reference values obtained from the work of Burchuladze et al. (Figure 3).

In the Jungfraujoch data, the residuals showed a coherent structure in the form of a wave with periodicity corresponding to that of the Hale cycle. In Mathematica, another instance of curve fitting was carried out with a sine wave, and a fit was found with $A = 2.228‰, \omega = 0.300$. The period is ≈ 21 years, and the amplitude is consistent with that found by Masuda et al. (Section 3.3.2). The obtained fit is depicted in Figure 9c of the appendix.

5.3 Final Residuals

The final residuals relative to the fits given in Table 6 (and in the case of Jungfraujoch after removing the Hale cycle) are depicted in the appendix for

Source	Time of extremum	Wolf number extremum type	Fit extremum type	Delay
Fruholmen	1976	minimum		
	1976.5	minimum		6.25
	1981.5	maximum		7.5
	1982.75		maximum	6.25
	1986.5	minimum		
	1989		minimum	7.5
Wellington	1972.75		maximum	
	1976.5	minimum		6.5
	1978		minimum	
	1981.5	maximum		6.75
	1983		maximum	6.5
	1986.5	minimum		
	1988.25		minimum	6.75
Jungfraujoch	1988		maximum	
	1989.5-1991.	maximum		3
	1993.5		minimum	3
	1996.5	minimum		2.5
	1999		maximum	2.5
	2000.5	maximum		4.5
	2004.5		minimum	4.5
	2008.5	minimum		1.5
	2010		maximum	1.5
	2014.5	maximum		
Schauinsland	1978		maximum	
	1981.5	maximum		2.5
	1984		minimum	2.5
	1986.5	minimum		3.75
	1989.5-1991.	maximum		
	1990.25		maximum	3.75
Burchuladze [21]	1913	minimum		3
	1916		maximum	3
	1917	maximum		3
	1919-1921		minimum	3
	1923-1923.5	minimum		5
	1926-1928		maximum	5
	1928	maximum		
	1931-1934		minimum	
	1933	minimum		4
	1936-1938		maximum	4

Table 7: Peaks and troughs in the Wolf number and the solar component of the found fits. A maximum/minimum in solar activity corresponds to a minimum/maximum in radiocarbon (respectively). A found extremum in sunspots was matched with the next corresponding extremum in ^{14}C levels: the found delay is given in the last column (the matched colours indicate corresponding extrema). The values were read from Figure 2. For comparison, values from Figure 3, obtained from the work of Burchuladze et al. are also given.

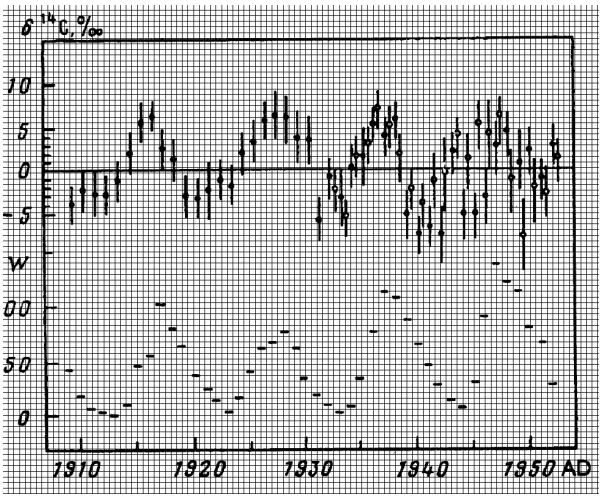

Figure 3: The Wolf number and the radiocarbon values obtained from Slovakian tree-rings and Georgian wines in the work of Burchuladze et al. This graph was copied from the paper in question ([21], Figure 3), and edited for better readability; namely a grid was added, with the spacing chosen such that a single grid interval corresponds to half a year on the horizontal axis.

each dataset separately. Figures 4 and 5 show the residuals for all datasets in a single graph and the most extreme values of all obtained residuals in terms of standard deviations, respectively. The following features can be noted:

- The Schauinsland and Vermunt sets show a very similar residual structure. This can be explained by their proximity: the sites are both high-altitude clean air stations in the Alps, somewhat less than 300 kms apart, and we expect to obtain almost identical values. Note that there is a shared wiggle in the residuals where both measurement series are present (peaking in 1978, then forming a small trough in 1980). The Vermunt dataset also shows a residual peak in 1971. The changes appear to be wave-like in shape, rather than sharp peaks, and it can be assumed that they are unfiltered harmonics in the Sun's magnetic cycle. It's noteworthy that the Vermunt set showed a very strong 6.7 year periodicity: the best single sine fit obtained in Mathematica actually had $\omega = 0.936$ and a large amplitude of 11.994 ‰. While this was discarded in favour of the seasonal fit (third best), it is in no way unphysical. The magnetic activity of the Sun has been shown to consist of several harmonics. For example, Kocharov et al. [29] found (through DFT) peaks at 5.5 year and 6.7 year periods. The latter was less pronounced and the authors claimed that it likely arised from noise, while not excluding the possibility that it is another harmonic of the Hale cycle. We do not take a stand on the matter, as in this project frequency analysis was not performed, only fitting, and it is

entirely possible that the obtained fit results from a combination of other harmonics. Nevertheless, it is a periodic variation, possibly emerging from the magnetic cycle of the Sun, which seems to be more pronounced in the given time interval. It is also present in the Wellington set. Double fits can also be obtained for these sets, showing independence from the other periodicities. The values marked with asterisks in Table 6 describe the fits in question; note that these are not the fits used in Figures 4 and 5, instead Table 8 in the appendix shows how the most extreme values would have changed in terms of sigmas had we used the double fits. The differences are minute and none of our conclusions are affected.

- Both for Vermunt and Schauinsland, a sharp peak of a single data point can be observed in the spring of 1979. For Vermunt, it's a jump of 54 ‰ (with respect to the previous data point) for the measurement period 16-03-1979 to 25-03-1979. For Schauinsland, it's a 60 ‰ jump in a measurement from 08-05-1979 to 21-05-1979. Other stations measuring at the time were Fruholmen and Wellington, neither of them show similar peaks. The origin of these peaks was not determined. It should be noted however that they are remarkably close to the SGR burst of 05-03-1979 [30]. If one considers the SGR as a possible source, the lack of evidence in the other datasets could be explained by a significant difference in altitude above sea level. The matter would be further complicated by the fact that the SGR originated from the Large Magellanic Cloud, and wouldn't have struck the Northern Hemisphere directly. As the two stations affected are close, an anthropogenic source is also possible.

- The Fruholmen set shows a jump of 66 ‰ between the measurements made from 29-03-1971 to 05-04-1971 and 26-04-1971 to 03-05-1971. Opposed to the 1979 peak, this jump in radiocarbon levels is not only for a single data point. The four residual data points before the jump are consistently low (all in the -27 to -40 ‰ range) and the four values after are consistently high (27 to 45 ‰ range).

- The Wellington residuals show four very large values from 1981 to 1983. These are 57.3, 84.7, 130.2 and 159.0 ‰, not consecutive. They are likely measurement errors, as otherwise such extreme peaks should have an obvious cause, be persistent, and be detectable in other measurement series.

5.4 Summary

In this project, radiocarbon data from the second half of the 20th century and the 21st century was analyzed. Through fitting a simple quadratic function plus sine waves, the bomb curve was eliminated along with periodic variations corresponding to the Sun's magnetic cycle or seasonal changes (where found). A set of residuals was produced and examined for peaks based on the standard deviations of the respective datasets. Significant jumps were found in the spring

of 1979 for two measurement sites (Vermunt, Schauinsland), and in 1971 for one site (Fruholmen).
The offset between the 11 year Schwabe cycle and the solar components of the obtained fits was examined, yielding average delays of 6.9 years (Fruholmen), 6.6 years (Wellington), 2.9 years (Jungfraujoch) and 3.1 years (Schauinsland).
The nominally 22 year periodicity of the Hale cycle was found in the Jungfraujoch dataset. Furthermore an approximately 6.5 year periodicity was found in the data from Wellington and Vermunt.
For all obtained sine fits, we presented the amplitudes and angular frequencies.

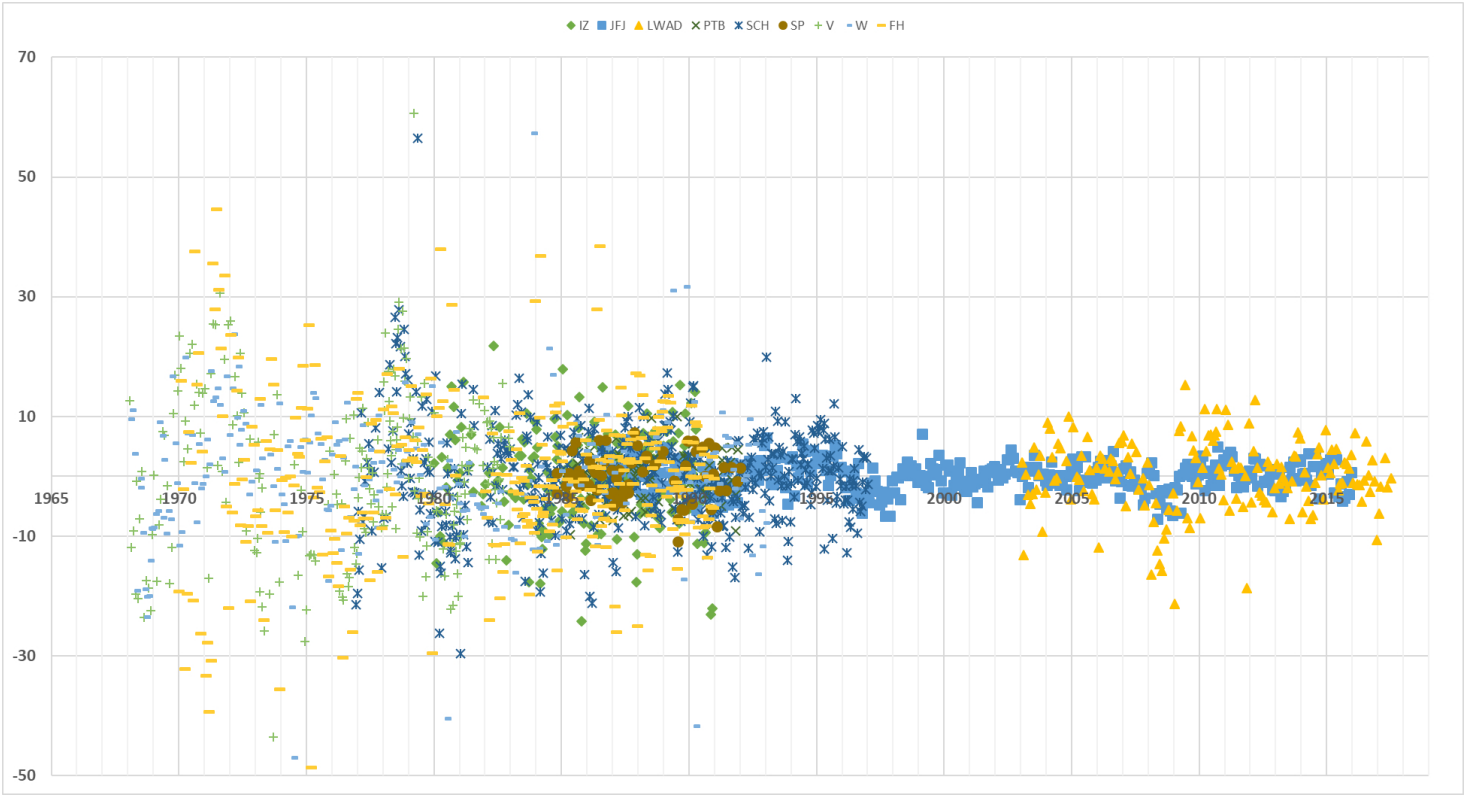

Figure 4: Final residuals from all datasets (some values from Wellington are not shown because of their extreme magnitude). The horizontal axis shows the time, the vertical is the Δ14C or D14C residual (‰).

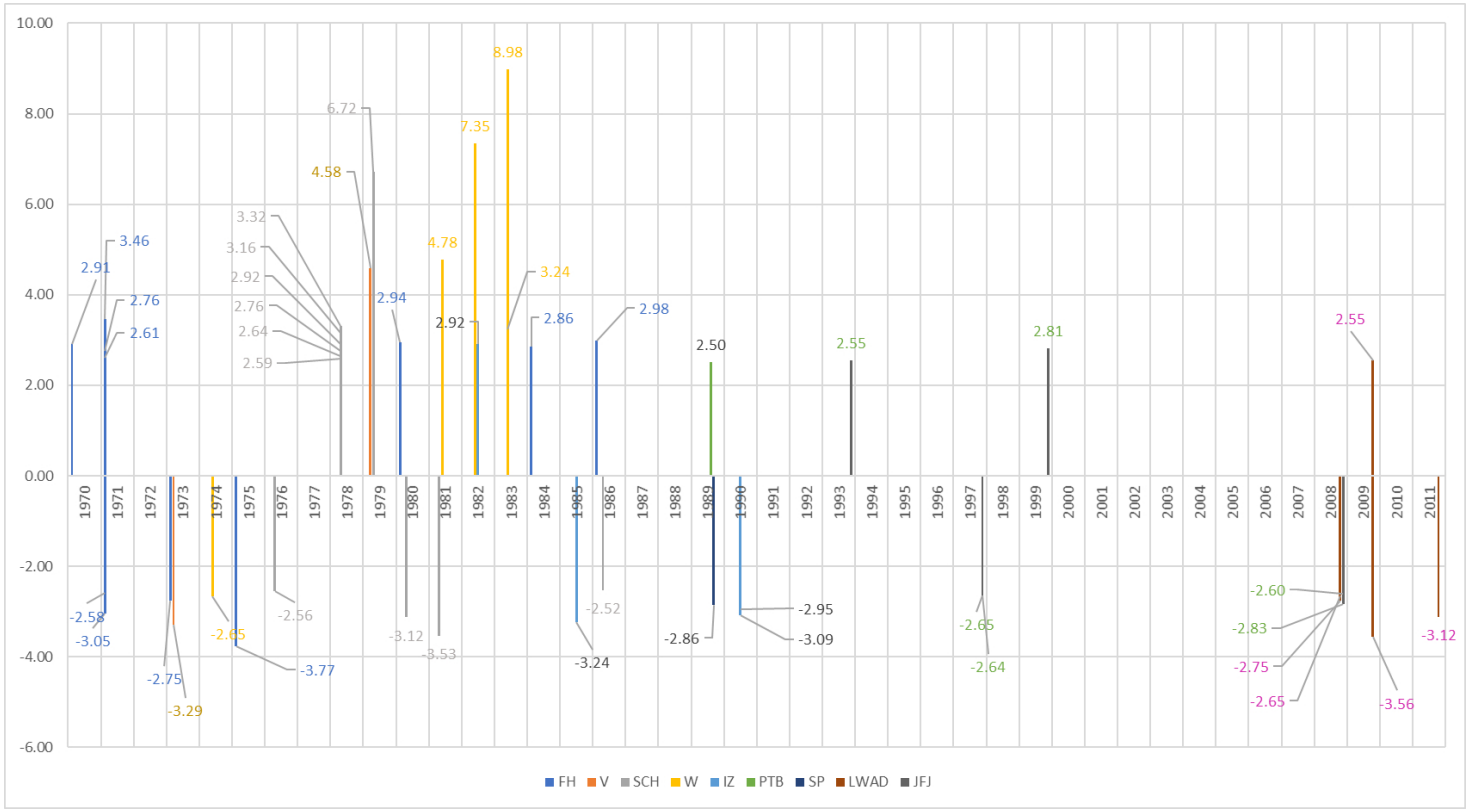

Figure 5: Final residuals from all datasets in terms of the sigmas of the respective datasets. Only the values exceeding 2.5 are shown.

6 Discussion and Conclusions

6.1 Discussion

The three main limiting factors in this analysis were the scope of the project, the quality and quantity of available data, and the complexity of the subject.
Because of the limited scope of the project, the data analysis was carried out in a simple, straightforward manner, using only one approach (curve fitting). We did not attempt to fit more than two sine waves to any dataset. The one exception is Jungfraujoch, where the residuals showed obvious structure, and even in that case the third wave was fitted on the residual set, not in combination with the other two. Combining sine waves is generally a better approach as the other components are also slightly affected and hence the results differ somewhat, but doing so would also increase computational and code complexity. A more general approach would be starting with frequency analysis and finding all the harmonics. Furthermore sine waves are only rough approximations for the shapes of the periodic changes in solar activity. It is known for example that the magnetic polarity of the Sun (alternating with the Hale cycle) affects the shape of the neutron flux curve, causing flat-top curves for one polarity and sharp peaks for the other [28]. More sophisticated periodic functions could lead to better fits.
The number of available datasets was limited. For the 21st century for example, only 2 sets were available, from sites close to each other. It is reasonable to assume that access to more data would have given a more complete picture. In the case of the 1979 peak, two out of four sets show an anomaly. Geographic proximity could be the reason, but one also has to consider the difference in altitudes (the stations where the peak was detected are both high altitude, the other two are both low altitude). With the methods used and the lack of further data it was not possible to reach a conclusion as to the origin of these patterns. It is noteworthy that older data has significantly larger measurement errors. 8-10 ‰ errors used to be common, while for the modern measurements these are around 2-4 ‰. Thus older results are in general less reliable.
Last but not least finding events of cosmic origin in the data, unless they (almost) instantaneously cause peaks would be an enormous undertaking because of the theoretical complexity of the matter. It would require modeling of the generation and dispersion of radiocarbon in all atmospheric layers to estimate how long it should take to observe radiocarbon changes after a certain event. The residuals were checked against the largest solar events from 1978 and no obvious connections (i.e. very large peaks with reasonably short delays) were found. This is not surprising considering the past unsuccessful attempts to detect the Carrington event in radiocarbon.

6.2 Conclusions

Analysis of atomic age radiocarbon data was carried out by curve fitting and examination of the obtained residuals for nine datasets. Fits corresponding to

the Schwabe cycle were found in four cases, and the Hale cycle was observed in one case. The amplitudes were in agreement with literature values.
The phase delays between the Schwabe cycle and the corresponding periodicities in radiocarbon levels showed significant differences between stations, with average delays ranging from 2.9 to 6.9 years. Similar inconsistencies can be found in the relevant literature.
An approximately 6.5 year periodicity was found in the data from two stations (Wellington and Vermunt), the origin of which is has not been conclusively determined. It is conjectured that this is a harmonic of the magnetic periodicity of the Sun.
Peaks were found in the radiocarbon levels in 1971 (Fruholmen) and 1979 (Vermunt and Schauinsland), with unknown origins. Some possible explanations were discussed.
Further research is needed to clarify the obtained results and provide the missing explanations. Based on the observations made in this project, it would be beneficial to focus on the difference between high-altitude and low-altitude measurements, and to obtain data which provides an even global coverage.

6.3 Acknowledgements

The author would like to thank Assistant Professor Michael Dee for his support and supervision, and Laurens Even for providing access to the Lutjewad dataset.

References

[1] E. A. G. Schuur, E. R. M. Druffel, and S. E. ed. Trumbore. *Radiocarbon and Climate Change: Mechanisms, Applications and Laboratory Techniques*. Switzerland: Springer International Publishing, 2016. DOI: DOI10.1007/978-3-319-25643-6.

[2] Sheridan Bowman. *Radiocarbon dating*. Vol. 1. Univ of California Press, 1995, pp. 9–15.

[3] Minze Stuiver and Henry A. Polach. "Discussion Reporting of 14C Data". In: *Radiocarbon* 19.03 (1977). 355, pp. 355–363. ISSN: 0033-8222. DOI: 10.1017/S0033822200003672.

[4] Willard F Libby. *Radiocarbon dating, Nobel Lecture*. Elsevier Publishing Company, 1964. URL: https://www.nobelprize.org/prizes/chemistry/1960/libby/lecture/ (visited on 05/19/2019).

[5] Ingeborg Levin, Tobias Naegler, Bernd Kromer, et al. "Observations and modelling of the global distribution and long-term trend of atmospheric 14CO2". In: *Tellus B: Chemical and Physical Meteorology* 62.1 (2010), pp. 26–46. DOI: 10.1111/j.1600-0889.2009.00446.x. eprint: https://doi.org/10.1111/j.1600-0889.2009.00446.x. URL: https://doi.org/10.1111/j.1600-0889.2009.00446.x.

[6] H.A.J. Meijer, M.H. Pertuisot, and J. van der Plicht. "High-accuracy C-14 measurements for atmospheric CO2 samples by AMS". In: *Radiocarbon* 48.3 (2006). Relation: https://www.rug.nl/ees/onderzoek/cio/index. Date submitted: 2008. Rights: University of Groningen, Centre for Isotope Research., pp. 355–372. ISSN: 0033-8222.

[7] Alex Bayliss, Gerry McCormac, and Hans van der Plicht. "An illustrated guide to measuring radiocarbon from archaeological samples". In: *Physics Education* 39.2 (Mar. 2004), pp. 137–144. DOI: 10.1088/0031-9120/39/2/001. URL: https://doi.org/10.1088%5C%2F0031-9120%5C%2F39%5C%2F2%5C%2F001.

[8] *Intcal Website*. URL: http://www.radiocarbon.org/IntCal13.htm (visited on 05/19/2019).

[9] *Intcal 13 Graphs*. URL: http://www.radiocarbon.org/IntCal13%20files/intcal13.pdf (visited on 05/19/2019).

[10] Fusa Miyake, Kentaro Nagaya, Kimiaki Masuda, et al. "A signature of cosmic-ray increase in ad 774-775 from tree rings in Japan". In: *Nature* 486 (June 2012). URL: https://doi.org/10.1038/nature11123.

[11] D. Güttler, F. Adolphi, J. Beer, et al. "Rapid increase in cosmogenic 14C in AD 775 measured in New Zealand kauri trees indicates short-lived increase in 14C production spanning both hemispheres". In: *Earth and Planetary Science Letters* 411 (2015), pp. 290–297. ISSN: 0012-821X. DOI: https://doi.org/10.1016/j.epsl.2014.11.048. URL: http://www.sciencedirect.com/science/article/pii/S0012821X14007481.

[12] Fusa Miyake, Kimiaki Masuda, and Toshio Nakamura. "Another rapid event in the carbon-14 content of tree rings". In: *Nature Communications* 4 (Apr. 2013). URL: https://doi.org/10.1038/ncomms2783.

[13] Fusa Miyake, Kimiaki Masuda, Masataka Hakozaki, et al. "Verification of the Cosmic-Ray Event in AD 993–994 by Using a Japanese Hinoki Tree". In: *Radiocarbon* 56.3 (2014), pp. 1189–1194. DOI: 10.2458/56.17769.

[14] Ulf Büntgen, Lukas Wacker, J Diego Galván, et al. "Tree rings reveal globally coherent signature of cosmogenic radiocarbon events in 774 and 993 CE". In: *Nature communications* 9.1 (2018), p. 3605.

[15] Hans E. Suess. "Radiocarbon Concentration in Modern Wood". In: *Science* 122.3166 (1955), pp. 415–417. ISSN: 00368075, 10959203. URL: http://www.jstor.org/stable/1751568.

[16] S. M. Chitre. "Overview of Solar Physics". In: *Lectures on Solar Physics*. Ed. by H. M. Antia, Arvind Bhatnagar, and Peter Ulmschneider. Berlin, Heidelberg: Springer Berlin Heidelberg, 2003, pp. 1–26. ISBN: 978-3-540-36963-9. DOI: 10.1007/3-540-36963-5_1. URL: https://doi.org/10.1007/3-540-36963-5_1.

[17] D. M. Volobuev and N. G. Makarenko. "Radiocarbon version of 11-year variations in the interplanetary magnetic field since 1250". In: *Geomagnetism and Aeronomy* 55.7 (Dec. 2015), pp. 938–944. ISSN: 1555-645X. DOI: 10.1134/S0016793215070282. URL: https://doi.org/10.1134/S0016793215070282.

[18] Masuda K., Nagaya K., Miyahara H., et al. "Cosmogenic radiocarbon and the solar activity". In: *Journal of the Physical Society of Japan* 78.SUPPL. A (2009). 1, pp. 1–6. ISSN: 0031-9015. DOI: 10.1143/JPSJS.78SA.1.

[19] Ronny Friedrich, Bernd Kromer, Frank Sirocko, et al. "Annual 14C tree-ring data around 400 AD: mid- and high-latitude records". In: *Radiocarbon* (2019), pp. 1–12. DOI: 10.1017/RDC.2019.34.

[20] Pavel Povinec, A. A. Burchuladze, and S. V. Pagava. "Short-Term Variations in Radiocarbon Concentration with the 11-Year Solar Cycle". In: *Radiocarbon* 25.02 (1983). 259, pp. 259–266. ISSN: 0033-8222. DOI: 10.1017/S0033822200005555.

[21] A. A. Burchuladze, S. V. Pagava, G. I. Togonidze, et al. "Radiocarbon and 11-Year Variations of Cosmic Rays". In: *Radiocarbon* 35.03 (1993). 347, pp. 347–350. ISSN: 0033-8222. DOI: 10.1017/S0033822200060343.

[22] Dazhuang Zhou, Chi Wang, Binquan Zhang, et al. "Super solar particle event around AD775 was found". In: *Chinese Science Bulletin* 59.22 (Aug. 2014), pp. 2736–2742. ISSN: 1861-9541. DOI: 10.1007/s11434-014-0345-z. URL: https://doi.org/10.1007/s11434-014-0345-z.

[23] Fusa Miyake, Kimiaki Masuda, Toshio Nakamura, et al. "Search for Annual 14C Excursions in the Past". In: *Radiocarbon* 59.2 (2017), pp. 315–320. DOI: 10.1017/RDC.2016.54.

[24] Ralph Neuhaeuser and V Hambaryan. "A solar super-flare as cause for the 14C variation in AD 774/5 ?" In: *Astronomische Nachrichten* 335 (Nov. 2014). DOI: 10.1002/asna.201412071.

[25] URL: https://cdiac.ess-dive.lbl.gov/ (visited on 05/11/2019).

[26] *Station Lutjewad Description*. URL: https://www.rug.nl/research/centre-for-isotope-research/research-and-projects/main-research/carbon-cycle-atmosphere/lutjewad/ (visited on 05/30/2019).

[27] URL: https://reference.wolfram.com/language/ref/FindFit.html (visited on 05/15/2019).

[28] B. Heber, H. Fichtner, and K. Scherer. "Solar and Heliospheric Modulation of Galactic Cosmic Rays". In: *Space Science Reviews* 125.1 (Aug. 2006), pp. 81–93. ISSN: 1572-9672. DOI: 10.1007/s11214-006-9048-3. URL: https://doi.org/10.1007/s11214-006-9048-3.

[29] G. E. Kocharov, V. M. Ostryakov, A. N. Peristykh, et al. "Radiocarbon content variations and Maunder Minimum of solar activity". In: *Solar Physics* 159.2 (July 1995), pp. 381–391. ISSN: 1573-093X. DOI: 10.1007/BF00686539. URL: https://doi.org/10.1007/BF00686539.

[30] T. L. Cline. "The unique cosmic event of 1979 March 5". In: *Comments on Astrophysics* 9 (1980), pp. 13–21.

7 Appendix

Here the results are presented graphically. For each data set, three relevant plots were created in Mathematica.

1. The fitted curve plotted on the set of data points. In these graphs the outliers (data points removed for the fitting) are not shown. The horizontal axis shows time in years, the vertical axis shows ^{14}C values in ‰. Refer to Table 5 to see whether a dataset consists of D14C or Δ14C values.

2. The list of the sums of the residuals-squared obtained in Mathematica is presented. Using this, one can qualify the goodness of a fit compared to that of others for the same dataset. The horizontal axis is just an index identifying the fit in Mathematica, and the vertical axis is dimensionless. The point corresponding to the used fit is given in the captions, in the form (x/n), where x is the position of the fit compared to the lowest (1 denoting the lowest point), and n is the total number of obtained fits.

3. The final residuals with respect to the fitted curve. This set now includes all data points, even those that were temporarily discarded as possible outliers. The vertical axis presents D14C or Δ14C values (‰) as before.

For Jungfraujoch, an extra graph was obtained (fitting of the Hale cycle). For Vermunt and Wellington, the found 6.5 year periodicities are also plotted.

Site	Date	Original residual	Original significance	New residual	New significance
W	1974.43	-47.0	2.7		< 2.5
	1981.35	84.7	4.8	90.9	5.1
	1982.25	130.2	7.3	134.7	7.6
	1983.38	159.0	9.0	158.2	8.9
	1983.83	57.3	3.2	54.6	3.1
V	1973.72	-43.6	3.3	-32.1	2.9
	1979.22	60.7	4.6	55.9	5.0

Table 8: Changes in the most extreme residuals of Wellington and Vermunt when a double sine fit (including the approximately 6.5 year periodicity) is used instead of the single sine fit. Significance is given in terms of standard deviations.

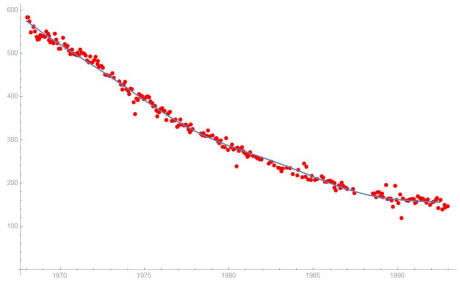

(a) The obtained fit.

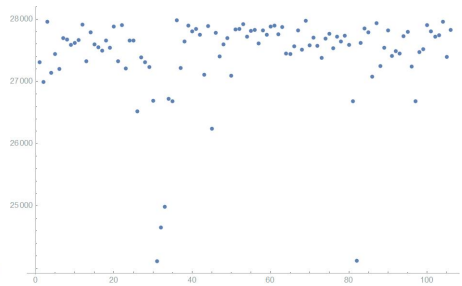

(b) Sums of the residuals squared for all the different fits obtained in Mathematica (3/106).

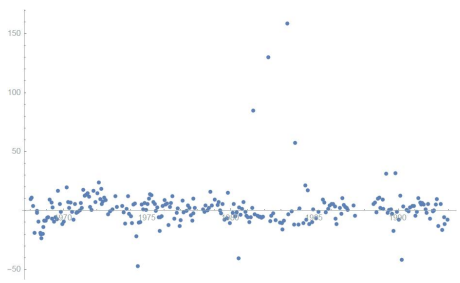

(c) Residuals with respect to the obtained fit.

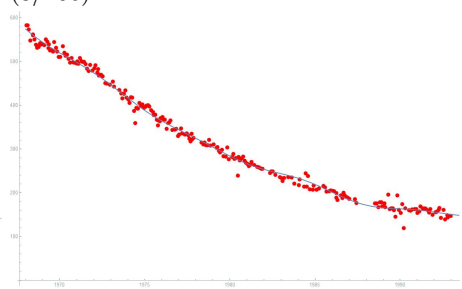

(d) Double fit obtained for Wellington (marked with an asterisk in Table 6).

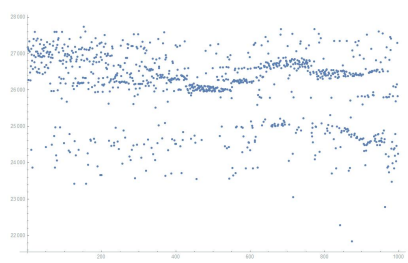

(e) Sums of the residuals squared for all the different double fits (3/998).

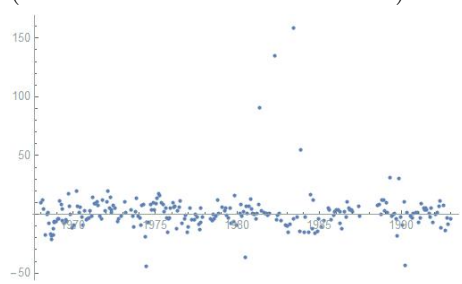

(f) Final residuals with respect to the double fit.

Figure 6: Results for Wellington.

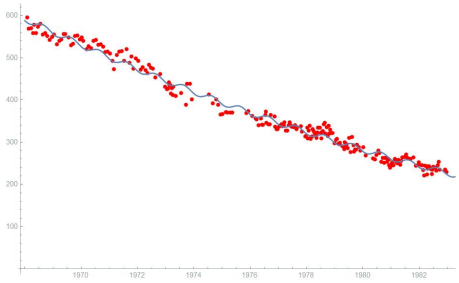

(a) The obtained fit.

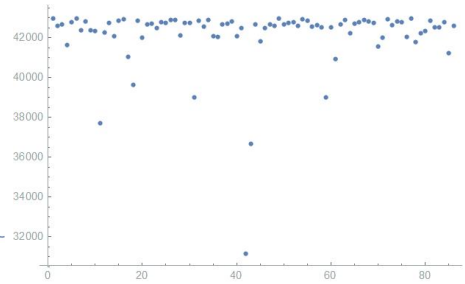

(b) Sums of the residuals squared for all the different fits obtained in Mathematica (3/86).

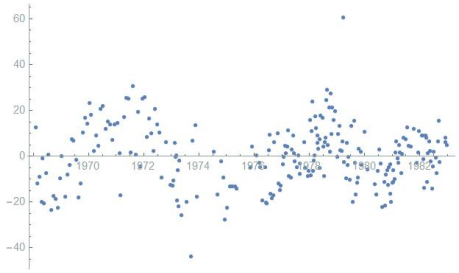

(c) Residuals with respect to the obtained fit.

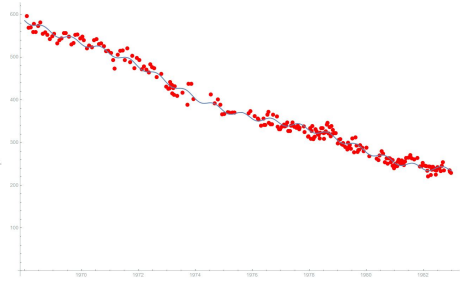

(d) Double fit obtained for Vermunt (marked with an asterisk in Table 6).

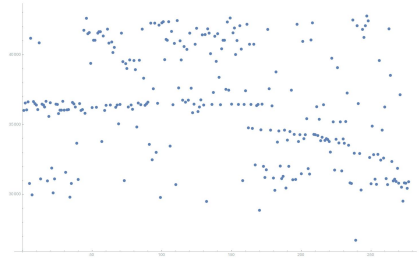

(e) Sums of the residuals squared for all the different double fits (1/277).

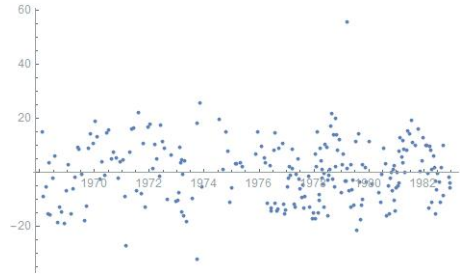

(f) Final residuals with respect to the double fit.

Figure 7: Results for Vermunt.

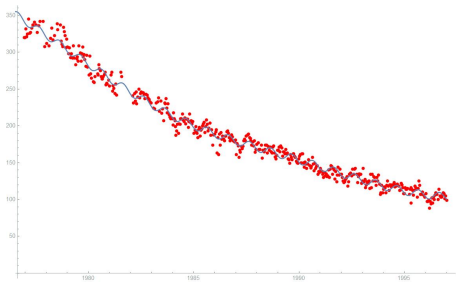

(a) The obtained fit.

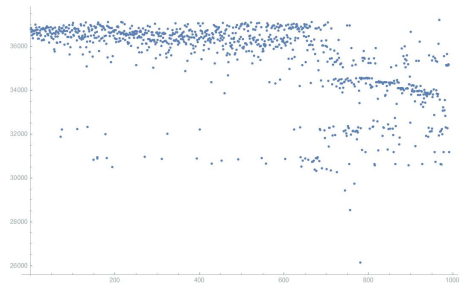

(b) Sums of the residuals squared for all the different fits obtained in Mathematica (1/991).

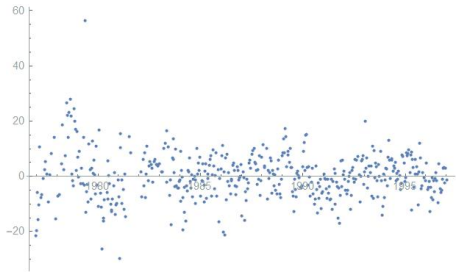

(c) Residuals with respect to the obtained fit.

Figure 8: Results for Schauinsland.

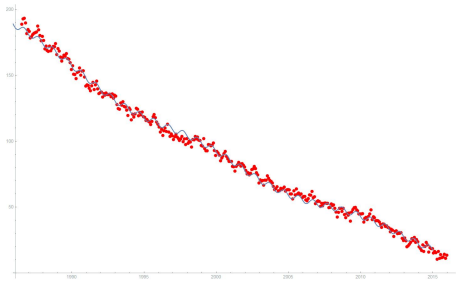

(a) The obtained fit.

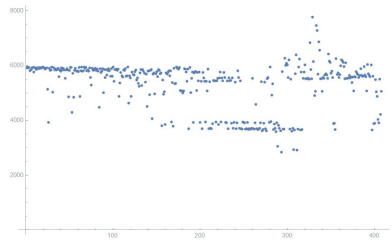

(b) Sums of the residuals squared for all the different fits obtained in Mathematica (4/408).

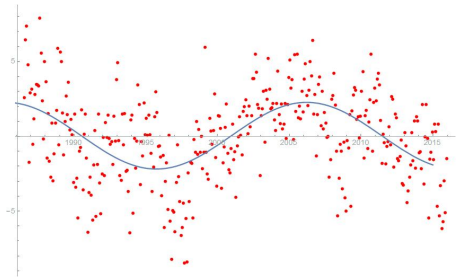

(c) Residuals with respect to the obtained fit, with a fitted sine wave (corresponding to the Hale cycle).

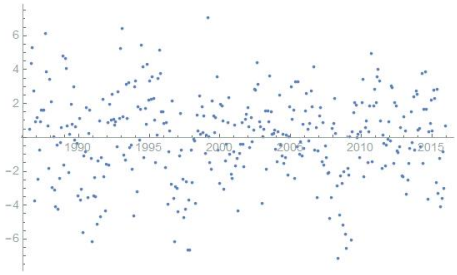

(d) Final residuals with respect to the Hale cycle fit.

Figure 9: Results for Jungfraujoch.

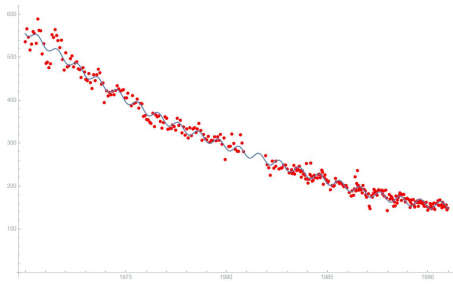

(a) The obtained fit.

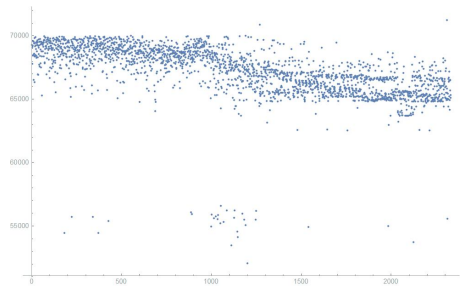

(b) Sums of the residuals squared for all the different fits obtained in Mathematica (1/2331).

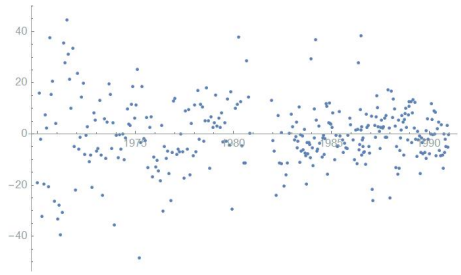

(c) Residuals with respect to the obtained fit.

Figure 10: Results for Fruholmen.

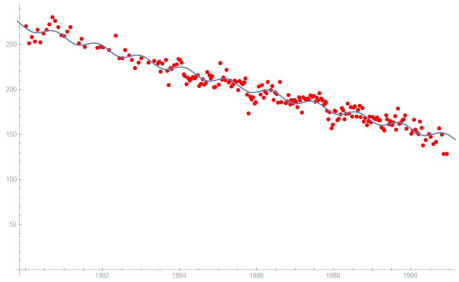

(a) The obtained fit.

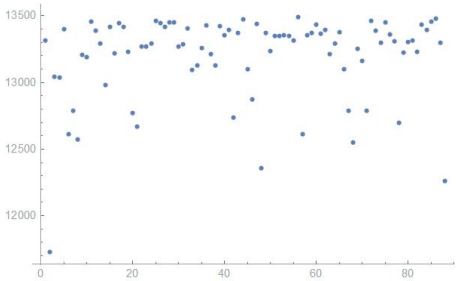

(b) Sums of the residuals squared for all the different fits obtained in Mathematica (1/88).

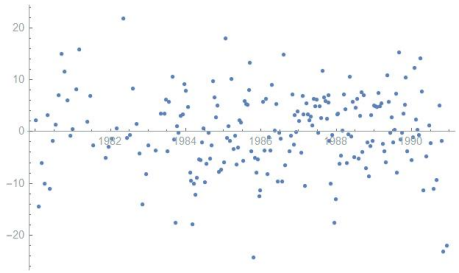

(c) Residuals with respect to the obtained fit.

Figure 11: Results for Izaña.

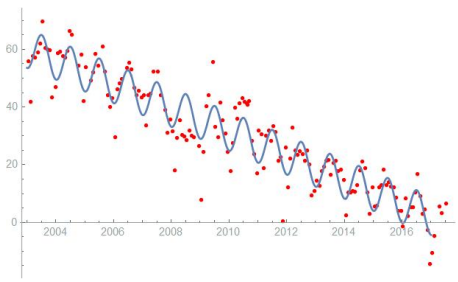

(a) The obtained fit.

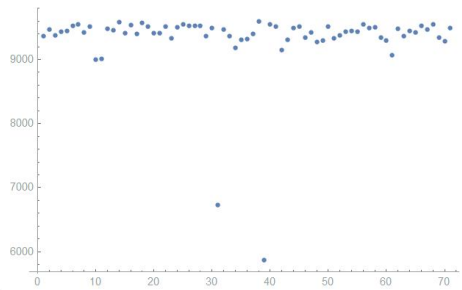

(b) Sums of the residuals squared for all the different fits obtained in Mathematica (1/71).

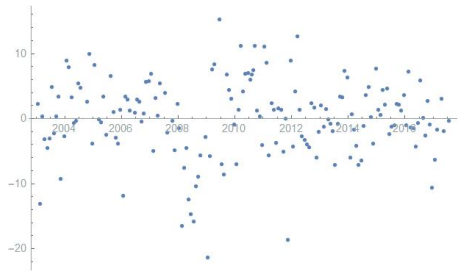

(c) Residuals with respect to the obtained fit.

Figure 12: Results for Lutjewad.

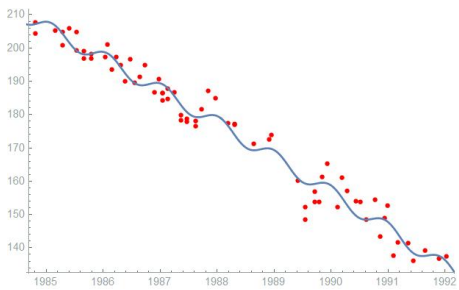

(a) The obtained fit.

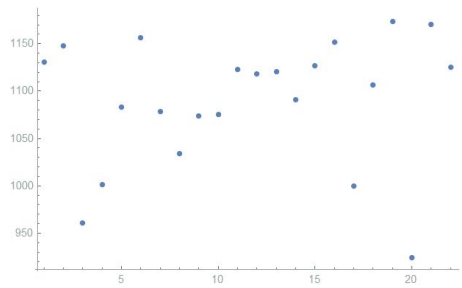

(b) Sums of the residuals squared for all the different fits obtained in Mathematica (4/22).

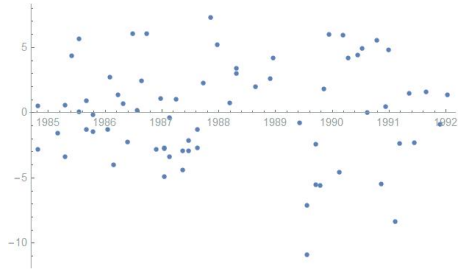

(c) Residuals with respect to the obtained fit.

Figure 13: Results for the South Pole.

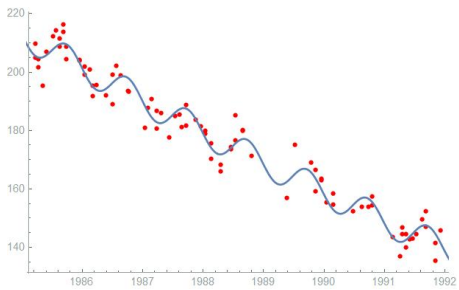

(a) The obtained fit.

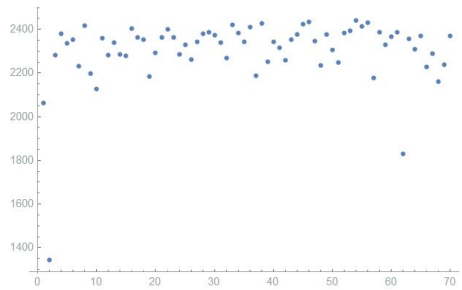

(b) Sums of the residuals squared for all the different fits obtained in Mathematica (1/70).

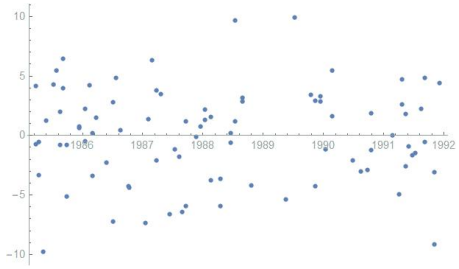

(c) Residuals with respect to the obtained fit.

Figure 14: Results for Point Barrow.